Chain Orientation and Defects in Lamellar Single Crystals of Syndiotactic Polypropylene Fractions

Wensheng Zhou,[†] Xin Weng,[†] Shi Jin,[†] Sanjay Rastogi,[‡] Andrew J. Lovinger,[§] Bernard Lotz,*[,⊥] and Stephen Z. D. Cheng*[,†]

Maurice Morton Institute and Department of Polymer Science, The University of Akron, Akron, Ohio 44325-3909; Eindhoven Polymer Laboratories, Eindhoven Technological University, NL-5600 MB Eindhoven, The Netherlands; Bell Laboratories, Lucent Technologies, Murray Hill, New Jersey 07974; and Institute Charles Sadron, 6 Rue Boussingault, Strasbourg 67083, France

Received June 6, 2003

ABSTRACT: Sectorization is frequently observed in elongated rectangular single crystals of syndiotactic polypropylene (s-PP) grown from the melt in thin films. The crystals are bound laterally by {100} and {010} growth planes. The constituent sectors are readily observed because of a difference in thicknesses; specifically, the sectors bound by the {100} planes [the (100) growth sectors] are thicker than those bounded by the {010} planes [the (010) growth sectors]. Dark field (DF) transmission electron microscopy (TEM) was utilized to examine the chain orientation and lattice defects in the different growth sectors of s-PP single crystals. The (020) DF images exhibited pairs of bright streaks that are more or less perpendicular to the (100) planes and cross over the whole width of the (100) sectors. In the (200) DF images, the (100) sectors also exhibited similar but dimmer streaks than those in the (020) DF images. This suggests that the crystal *c*-axis orientation in the (100) crystal sectors undergoes a periodic change in inclination along both the longitudinal (parallel to the *b*-axis) and the transverse axis (parallel to the *a*-axis) directions of the single crystal. The ripples in the (100) sectors, previously observed in TEM, were also seen with atomic force microscopy as sinusoidal-like periodic height changes along the longitudinal axis direction at both room temperature and high temperatures. This periodic height change accounted for the pairs of bright streaks in the (020) DF images. The ripple formation was explained by lamellar thickening in the (010) sectors during crystal growth. This thickening process causes lateral contractions, which accumulate mainly along the longitudinal axis direction of the single crystal. On the other hand, the (020) DF images exhibited a relatively uniform brightness in the (010) sectors, while in the (200) DF images, several dark zones in the (010) sectors were more or less along the diagonal directions of the single crystal. This observation indicates that the crystal *c*-axis in these zones is slightly deviated from the (200) planarity due possibly to the lateral contraction in the (010) sectors. A regular Moiré pattern in the (010) sectors was observed in the (020) DF images, and no Moiré patterns were found in the (100) sectors. Again, this was presumably due to sinusoidal-like ripples, which substantially affect the crystal plane orientation with respect to the lamellar crystal normal. In the (200) DF images, only random Moiré fringes could be found and, in particular, when the (010) and the (100) sectors overlapped. However, regular Moiré fringes were observed continuously over both sectors in (220) DF images.

Introduction

Studies over the past 15 years have shown that elongated rectangular lamellar single crystals of syndiotactic polypropylene (s-PP) can be grown isothermally from the melt in thin films.[1−9] These single crystals formed at high crystallization temperatures (T_c) possess an orthorhombic unit cell having antichiral helical chain packing along both the *a*- and *b*-axes (form III using the nomenclature of refs 1−5 or form I in recent literature[12,13]) based on electron diffraction (ED) and wide-angle X-ray diffraction experiments.[1−5,7−13] The symmetry is close to *Ibca*, and the unit cell dimensions are $a = 1.450$ nm, $b = 1.120$ nm, $c = 0.740$ nm, and $\alpha = \beta = \gamma = 90°$. In the low T_c range, packing defects are introduced into form III (using the earlier nomenclature). On the basis of the shape of the single crystals, the T_c-dependent crystal growth rates along both the [100] and [010] directions were highly anisotropic. The growth rate along the [010] direction (the long longitudinal axis) is around 1 order of magnitude faster than that along the [100] direction (the short transverse axis).[11] This leads to a large aspect ratio in the rectangular single-crystal shape with the *c*-axis parallel to the lamellar normal in a perfect s-PP single lamellar crystal. In the high T_c range ($T_c \geq 120$ °C), the lamellar single crystals frequently exhibit sectorization along both diagonals to form the (010) [with the (010) growth edge] and the (100) [with the (100) growth edge] sectors, which can be clearly observed under transmission electron microscopy (TEM) and atomic force microscopy (AFM).[5−8,11] This sectorization is evidenced by the thickness difference between these two sectors with the (100) sectors being thicker.

In-situ AFM results showed that the thickness difference between the two sectors was also dependent upon crystallization time (t_c). In the initial stages, the difference in thickness between the thick (100) sector and the thin (010) sectors could be more than 30%. With increasing t_c, the difference in thickness gradually decreased to less than 15% and then holds almost constant. This was mainly due to the thickening of the (010) growth sectors, while the thickness of the (100)

[†] The University of Akron.
[‡] Eindhoven Technological University.
[§] Lucent Technologies.
[⊥] Institute Charles Sadron.
* To whom correspondence should be addressed. E-mail: scheng@uakron.edu and lotz@ics.u-strasbg.fr.

10.1021/ma030312x CCC: $25.00
Published on Web 11/11/2003

sectors remained constant after the early stages of crystal growth.[11] Melting of the s-PP single crystals monitored by in-situ AFM revealed different melting paths for the (100) and (010) sectors. When single crystals isothermally grown at $T_c = 120$ °C were heated to 125 °C, the melting process began at separate spots located on the edges of the thick (100) sectors. These domains could "heal" via recrystallization if the samples were annealed at 125 °C for a long period of time. A further increase of temperature led to the melting of both sectors. Again, the melting of the thick (100) sectors started at apparently less stable spots along the (100) growth edges of the single crystals. In the (010) sectors, melting started at the free edges of the single crystals and progressed toward the inside of the sectors.[11]

Chain folding in the different sectors of the s-PP lamellar single crystals was studied with polyethylene (PE) decoration,[5,7] single-crystal deformation,[7] and folding energy calculation techniques.[14] It is generally understood that in the (100) sectors the chain folding is along the *b*-axis direction (the longitudinal axis direction) of the crystal.[5,7] In the (010) sectors, it has been speculated that the chain folding is along the ⟨110⟩ and/or the [100] directions.[5,7] If the chain folding behavior is truly different in these two sectors, one may explain the lamellar thickness difference between these two sectors by invoking a difference in surface free energies.[7,11]

In this publication, we specifically focus on, for the first time, the chain orientation in s-PP lamellar single crystals investigated using two different TEM dark field (DF) experimental techniques. It was deduced that the chain orientation in the (100) and (010) growth sectors are different. The streaks found in the (100) sectors of the DF images are associated with the ripples previously observed by TEM. The importance of this study lies in providing an explanation of the ripple formation mechanism in the (100) sectors, which is currently the subject of active discussion.[15] In addition, the DF images of superimposed s-PP lamellar single crystals show Moiré patterns, which enables probing of crystal defects. Interestingly, regular Moiré patterns can only be observed in the (010) sectors of the (020) DF images and in both of the (010) and (100) sectors of the (220) DF images. Only random fringes were found in the (010) sectors of the (200) DF images.

Experimental Section

Materials and Samples. The two s-PP fractions used in this study were provided by Phillips Petroleum Co. in Bartlesville, OK. Detailed molecular analyses were reported in previous publications.[9,10] These s-PP fractions had number-average molecular weights of 20 800 and 33 300 g/mol with a polydispersity of 1.1. The samples' syndiotactic regularity [r] (%) varied between 95% and 94%, the triads [rr] (%) between 93% and 92%, and the pentads [rrrr] between 88% and 86%, based on nuclear magnetic resonance measurements. In this study, we did not find any dependence of s-PP single crystal structure or morphology on molecular weight which is likely due to the similar molecular weights of the two samples. Therefore, we do not specifically distinguish the TEM and AFM observations obtained from these two samples.

Thin-film samples were prepared for TEM and AFM experiments by a solution-casting method (from xylene with a concentration of 0.1% (w/v)) on carbon-coated glass slide surfaces, and they had a thickness of about 20−50 nm. The remaining solvent was evaporated at high temperature in a vacuum. The thin films were heated to 180 °C and held there isothermally for 2 min in a hot stage (Mettler FP-80HT). The samples were then quickly transferred to another hot stage (Mettler FP-84HT) preset at an isothermal T_c. All the isothermal crystallization processes were conducted in a dry nitrogen atmosphere.

Instrumentation and Experiments. Single-crystal morphology was observed with a TEM (JEOL JEM-1200 IIX) at an accelerating voltage of 120 kV. After complete crystallization, the films were cooled to room temperature. The s-PP thin films were separated from the glass surface by immersing the samples into hydrofluoric acid. The samples were then floated on the surface of distilled water and picked up on copper grids to obtain bright field (BF) and DF images using TEM. There are two ways to obtain DF images. In the conventional technique, centered DF operation (CDF), the objective aperture remains centered while the main beam is tilted so that the selected diffracted beam goes through the objective aperture. CDF imaging minimizes aberrations and astigmatism, and the DF image is focused. In the less commonly used method, the multiple-image DF method [also named diffraction DF (DDF) method], the ED pattern is defocused by adjusting the intermediate lens current. Each defocused diffraction spot is a DF image corresponding to the Bragg reflection involved, while the center disk displays the BF image. This DDF method is particularly suitable for beam-sensitive materials like s-PP. The DDF technique enables strict comparison of the various dark field images associated with the whole pattern. It provides simultaneous views of the BF and DF images as well as all of the diffraction patterns having correct orientation with respect to the field. Furthermore, it gives an identical dose to the (*hk*0) diffractions in generating the DF images. The operation is easy, but the images are of low magnification. Also, the images are not perfectly focused, and the DF images may have aberrations since they are not on the optical axis.[16,17]

An AFM (Digital Instrument Nanoscope IIIA) was used to examine the surface topology of the s-PP single crystals on the glass substrates. A 100 μm scanner was selected, and tapping mode was used to obtain both height and phase images. The cantilever force was light enough to limit damage to the sample, yet heavy enough so that the surface features could be accurately explored. The scanning rate was 1−3 Hz for low-magnification images (512 × 512 pixels per image). Lamellar thickness was obtained through scans across the single crystals. An in-house-designed hot stage was coupled with the AFM, and the sample temperature was controlled between 30 and 180 °C. A thermocouple was used to detect the surface temperature of the samples, which remained stable to within ±1 °C.

Results and Discussion

Chain Orientation Determination in Single Crystals Based on DF Images. Figure 1 shows a BF image of part of a s-PP lamellar single crystal without metal shadowing. The image exhibits sectorization with a low contrast. The (100) sectors are darker and, therefore, thicker than the (010) sector, resulting in higher electron density. This is consistent with the previously reported AFM observations.[6,7] A DF image of a s-PP lamellar single crystal with similar sectorization is exhibited in Figure 2. This image was obtained using the (020) ED spot of the diffraction pattern shown in the inset of Figure 2. The bright streaks in Figure 2 resulted from the fact that in these streaks the *c*-axis orientation in the crystal satisfied the (020) diffraction condition, while in the dark areas the orientation departed from this condition. Bright streaks in the thick (100) sectors were observed to be more or less perpendicular to the longitudinal axis as already reported in ref 5. In most cases, two bright streaks were associated in pairs and merged at the inner edges of the sectors at the boundary between the (100) and (010) sectors. The streaks reveal a seemingly periodic *c*-axis orientation

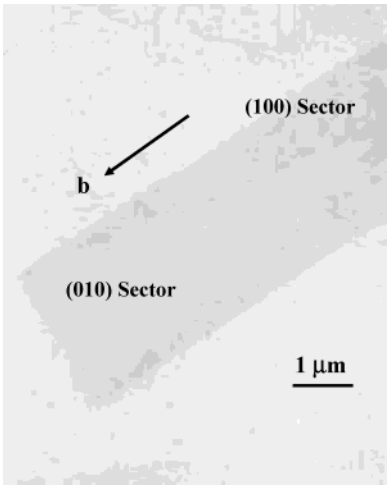

Figure 1. A BF image of an unshadowed s-PP lamellar single crystal with sectors having two different thicknesses grown from the melt at $T_c = 130$ °C.

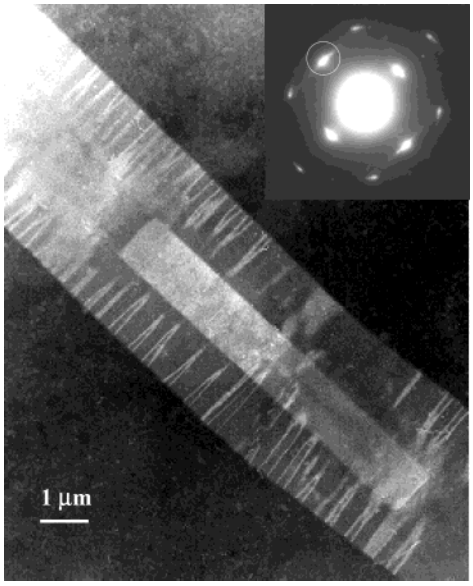

Figure 2. A (020) DF image of a s-PP lamellar single-crystal grown from the melt at $T_c = 130$ °C. Note that there is a small lamellar single-crystal overgrowth on the top of the large lamella. Since the contrast of some streaks is enhanced in the area of the overgrown crystal, the existing streaks may affect the growth of the overgrown single crystal. An ED pattern is inserted in correct orientation; the (020) diffraction spot is circled.

change in the crystal along the longitudinal axis direction in the (100) crystal sectors. The spacing of this periodicity was around 0.5 μm, as judged by the distance between the neighboring pairs of streaks.

The origin of this periodic crystal *c*-axis orientation change in the (100) sectors is being discussed. It was reported, on the basis of TEM observations, that the streaks were due to ripples (or bands of undulation) in the (100) sectors that are perpendicular to the longitudinal axis of the single crystal.[5] The periodicity of these ripples was almost identical to that of the streaks. In our experiments, we have also found these ripples in both TEM and AFM experiments. Figure 3 is an example of the ripples observed with the AFM at room temperature, which indeed correspond to periodic height changes of the (100) sector surfaces along the longitudinal axis direction, as shown in the height vs distance scan along this direction (included in Figure 3). Note

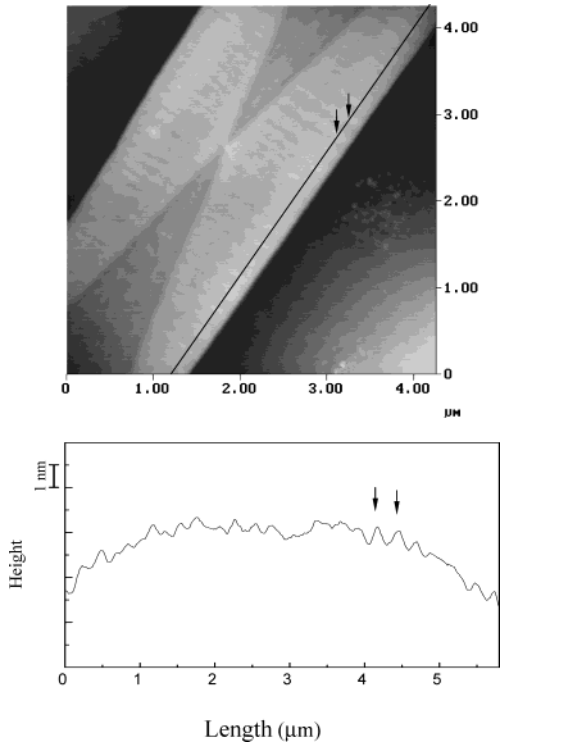

Figure 3. A room temperature AFM image of a s-PP lamellar single crystal showing the ripples in the (100) sectors. A height scan along the longitudinal axis (the *b*-axis) is also included. The crystal was grown at $T_c = 130$ °C from the melt in a thin film.

that the ripples are only found in the (100) sectors and not in the (010) sectors.

The formation of these ripples was associated with thermal stresses generated on cooling resulting from the anisotropic coefficients of thermal expansion (CTE) along the longitudinal axis (the *b*-axis in the crystal unit cell) and the transverse axis (the *a*-axis in the crystal unit cell) directions in s-PP lamellar single crystals.[5] Indeed, the CTE along the longitudinal axis direction is about 1 order of magnitude higher than that along the transverse axis direction.[5,10] Furthermore, the chain folding behavior could be different between the (100) and the (010) sectors, which might affect the chain orientation of these two types of sectors in these crystals.[5,7] If the folds are along the (200) planes, adjacent chains are only 0.56 nm apart, which corresponds to the tightest folds. Along the (020) planes, this distance is significantly larger (0.725 nm), and even more so along the (220) planes (0.93 nm).[14] Therefore, it was suggested that one needs to consider the balance of the shrinkage between the crystal core and the folds (including loops), which might act like stretched amorphous material during cooling. In the (010) sectors where the ripples are not formed, it was speculated that both the amorphous non-(200)-folds and the crystal core might exhibit comparable CTEs, leading to a contraction of the (010) sector along the longitudinal axis following a CTE of 10^{-4} during cooling.[5] However, in the (100) sectors, it was presumed that a very large shrinkage of the crystal core was opposed by a smaller shrinkage of the amorphous (200)-folds. As a result, a uniform macroscopic shrinkage might not take place during cooling, but rather, the crystals may deform by developing ripples.[5] These ripples would cause changes in the crystal plane orientations and deviation from the lamellar crystal normal and thus resulting in the observation

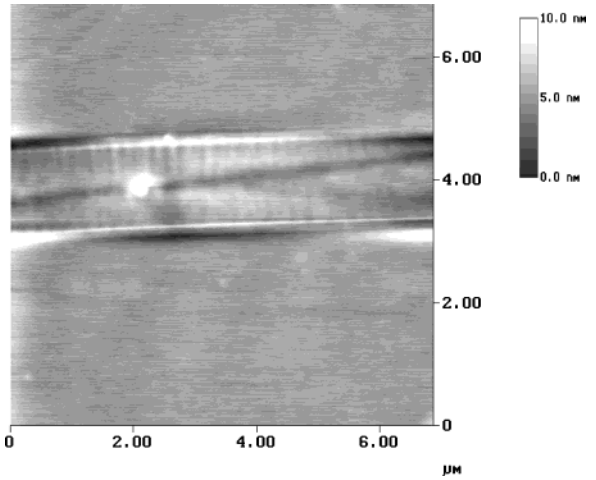

Figure 4. An AFM image of a s-PP lamellar single crystal showing the ripples in the (100) sectors at the crystallization temperature. This image is obtained at 120 °C.

of streaks in the DF images associated with periodic height changes.[5]

If anisotropic thermal shrinkage of the crystal were the sole reason for the experimental observations, the ripples should not be observed when the crystal is maintained at high temperatures. Correspondingly, the periodic height change along the longitudinal axis direction should disappear in AFM images at high temperatures. However, with the availability of a heated AFM stage now we have found that these transverse ripples can be observed even during crystallization at 120 °C, as shown in Figure 4. This demonstrates that the ripple formation is intrinsically associated with factors governing crystal growth *already at the* T_c. It also raises the question of the extent to which anisotropic CTE behavior and the compromise between the dimensional changes of the crystal core and amorphous layer of the (200)-folds in the (100) sectors contributes to the overall phenomenon. Preliminary observations (unpublished results) reveal amplitude differences between the rippling observed at the growth temperature and following cooling to ambient. We are investigating these differences and plan to report on them in the future.

One probable explanation of the ripple formation at high temperatures may lie in the thickening of the (010) sectors during crystal growth. We know that the thickness of the (100) sectors is constant after the initial growth, while the thickness of the (010) sectors increases continuously when the s-PP lamellar single crystals are grown from the melt in thin films.[11] To maintain a constant lateral area, new s-PP molten molecules are needed to join the single crystal. However, during crystal growth, molten s-PP molecules are most likely to diffuse to the crystal growth fronts and are less likely to diffuse underneath or on top of the crystal. Since the (010) sectors are bounded on two sides by the (100) sectors and only one edge in each sector is the growth front, the thickening of (010) sectors along the lamellar normal direction should generate lateral contractions if no new s-PP molecules are supplied. In this case, the overall contraction is along the longitudinal axis direction of the crystal given the anisotropic shape of the single crystal, and the largest lateral contraction is accumulated along the boundaries between the (100) and (010) sectors. Because of this anisotropic contraction, the ripples formed may periodically vary the

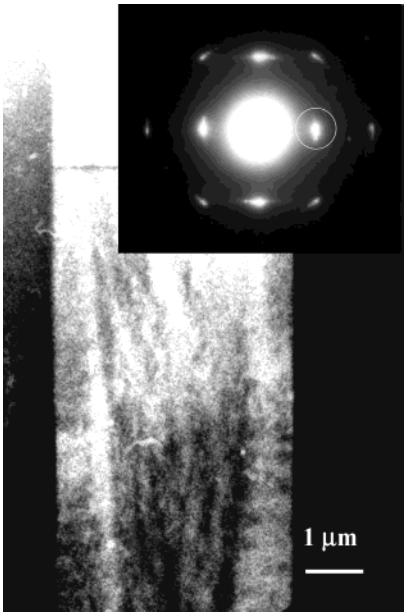

Figure 5. A (200) DF image of a s-PP lamellar single-crystal grown from the melt at T_c = 130 °C. An ED pattern is also inserted in correct orientation; the (200) diffraction spot is circled.

crystal *c*-axis orientation in the (100) crystal sectors. In the (020) DF images, this variation generates the visible streaks. A similar observation has been reported in the case of isotactic poly(2-vinylpyridine) in which the frustrated structure allows thickening only in every other sector of a hexagonally shaped single crystal.[18] In that case the thickened sector contracts and remains flat, whereas the nonthickened one forms ripples.

Now turning our attention to the (010) sectors, we find that Figure 2 does not show any streaks in these sectors; instead, only a relatively uniform low brightness can be seen, which is consistent with the AFM observations in Figures 3a and 4. This observation indicates that in the (010) sectors the crystal *c*-axis in the (020) crystal planes may also slightly deviate from the lamellar surface normal. However, the amount of tilt and its orientation in the (010) sectors cannot be obtained solely on the basis of the (020) DF images.

Figure 5 shows a (200) DF image of a s-PP single crystal. In the (100) sectors, a weak modulation of the intensity along the longitudinal axis direction can be seen, meaning that the observed ripples also affect the crystal *c*-axis orientation in the (200) planes, which thus deviates from the lamellar normal. Combined with the observations of (100) sectors in the (020) DF image in Figure 2, we can conclude that the crystal *c*-axis orientation in (100) sectors has periodic variations in inclination relative to the lamellar normal along both of the longitudinal and transverse axis directions and, possibly, the primary inclination variation being along the longitudinal axis direction. Some dark zones, more or less along the diagonal directions, can also be observed in the (010) sectors. They may be considered as additional evidence for lateral contractions in these sectors. This must lead to deviations of the crystal *c*-axis orientation from the lamellar normal (see below results from our DDF image).

In the normal DF imaging technique only one of the diffracted beams is used to form the image. A better way to study crystal morphology involves comparing DF images obtained simultaneously from different (*hk*0)

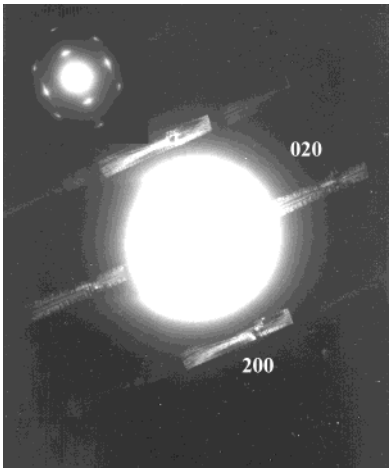

Figure 6. A DDF DF image of a s-PP lamellar single-crystal grown from the melt at T_c = 130 °C. An ED pattern is also inserted in correct orientation.

diffracted beams of the same crystal with the same dose. Figure 6 shows a DDF image of a s-PP single crystal. Both the (020) and (200) DDF images exhibit bright streaks perpendicular to the longitudinal axis in the (100) sectors. In the (200) DDF images, bright zones along the diagonal direction in the (010) sector are also observed. These features of the different DDF images are similar to those in Figures 2 and 5 using the conventional DF technique. The bright streaks in the (100) sectors of the (200) DDF are more evident than in the conventional DF image shown in Figure 5 and allow direct comparison with those in the (010) sectors.

Moiré Patterns in Multiple-Layer Lamellar Single Crystals. Moiré patterns are widely observed in polymer single crystals in TEM DF images when lamellar crystals are superimposed.[19−21] There are two fundamentally different types of Moiré interference: translation (due to the spacing difference between two sets of parallel crystal planes) and rotation (due to the rotation of two sets of crystal planes with the same spacing).[22,23] The type of Moiré pattern and the corresponding parameters (the rotation angle or the spacing difference) can be calculated from the pattern direction and the spacing between fringes.

Figures 7a and 8 show two sets of Moiré patterns in our DF images; Figure 7b is the TEM BF image of Figure 7a, which does not show any fringe due to the very low diffracted intensity and serves as a reference. The Moiré pattern obtained from the (200) DF image (Figure 7a) exhibits regular parallel fringes in the (010) growth sector. Very few defects can be observed (see the arrow in the figure pointing to a dislocation caused by inserting or losing a (200) plane into the lattice). Only at the upper left corner are there clear irregular fringes which corresponds to the region which is probably resulted from lamellar bending. Since the interference was regularly perpendicular to the (200) planes in the crystals, this Moiré pattern was formed by a rotation of two sets of (200) planes of the lamellar single crystals. With d being the spacing between (200) planes (0.725 nm), and D the spacing of neighboring fringes (83 nm), the rotation angle can be calculated on the basis of the equation $D = d/(2 \sin \alpha/2) \approx d/\alpha$, and $\alpha \approx 0.8°$. It is interesting that in Figure 7a no Moiré fringes are observed in the (100) sectors. This may likely be due to the ripples in the (100) growth sectors that periodically changed the crystal c-axis orientation along both the longitudinal and transverse axis directions and led to the disappearance of the fringes. Therefore, slightly different crystal c-axis orientations in these two sectors could significantly affect the ability to form Moiré patterns.

On the other hand, the Moiré pattern obtained from the (020) DF image in Figure 8 exhibited seemingly random fringes at the center part of the figure generated by two superimposed lamellar single crystals. Only in a few local parts were fringes observed (see arrows in this figure). It is noteworthy that these regular fringes are observed in the overlapped (100) sectors (the white arrow) and in the overlapped (010) sectors (the black arrow), while major areas show more randomized fringes in these two superimposed lamellae, particularly where the (010) sector of one crystal with the (100) sector of another overlapped each other. This indicates

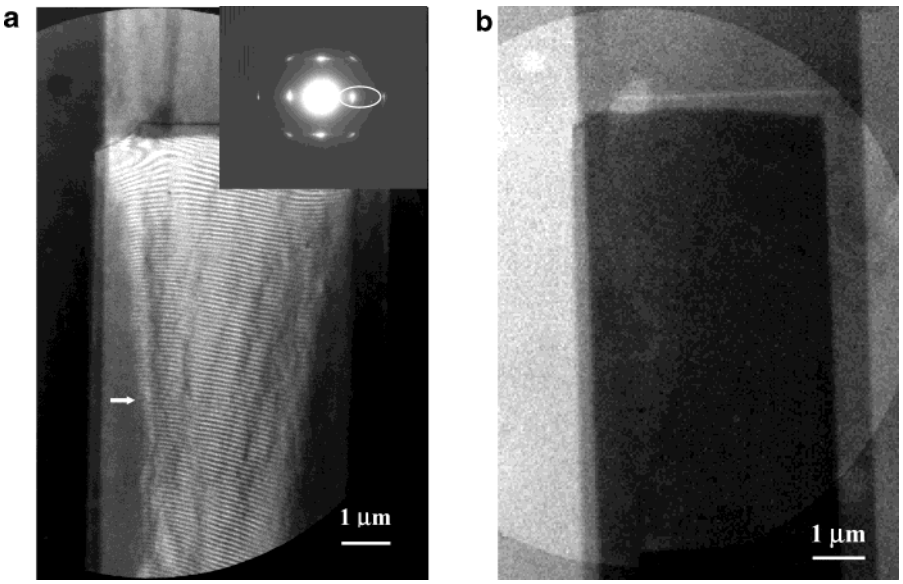

Figure 7. A (200) DF Moiré pattern observed from two s-PP lamellae superposed onto each other. The lamellar single crystals were grown at 130 °C. An ED pattern is also inserted in correct orientation. The (200) diffraction spot is circled in (a). The corresponding BF image is also included in (b). On the top of the Moiré pattern in (a) this is a dark line which is a streak of the crystal. This streak can also be recognized in (b) as a bright line on the top of the figure.

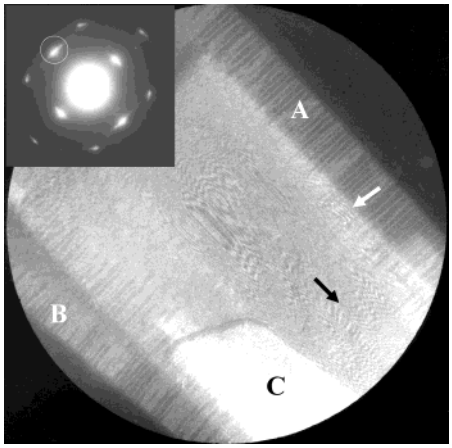

Figure 8. A (020) DF Moiré pattern observed from several s-PP lamellae superposed onto each other. The lamellar single crystals were grown at 130 °C. An ED pattern is also inserted in correct orientation. The (020) diffraction spot is circled.

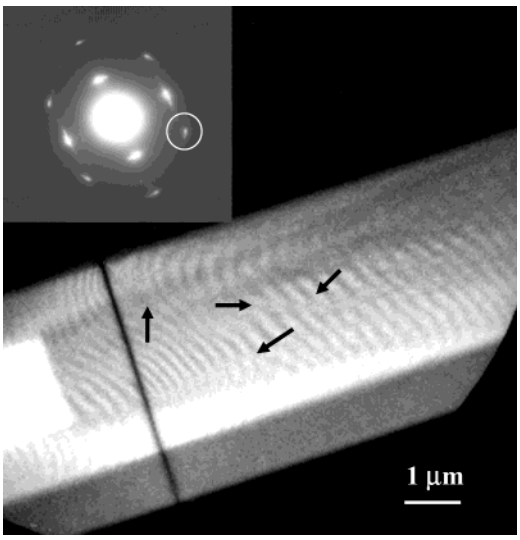

Figure 9. A (220) Moiré pattern observed from several s-PP lamellae superposed onto each other. The lamellar single crystals were grown at 130 °C. An ED pattern is also inserted in correct orientation. The (220) diffraction spot is circled.

again that the crystal *c*-axis orientation variations in the (100) sectors and the lateral contractions in the (010) sectors did significantly affect the observed Moiré fringes. Note that in this figure two crystals were superimposed onto each other across most of the area. In a small region at the bottom (area C in the figure) three lamellar crystals were superimposed onto each other. However, for both crystals, certain parts along the longitudinal edges (along the *b*-axis direction) remain uncovered (areas A and B in the figure; note that A and B belong to different single crystals). In these two areas, only bright streaks were found similar to those observed in the (020) DF images (as seen in Figure 2). Combined with the observations in Figures 7a and 8, it suggests that the inclination of the crystal *c*-axis from the lamellar normal in the (010) sectors may be mainly toward the longitudinal axis direction of the single crystal.

An extensive Moiré pattern was observed in a (220) DF image, as shown in Figure 9. Interestingly, the fringes were observed continuously across both of the (100) and (010) sectors. This illustrates that in both growth sectors the (110) plane orientation with respect to the lamellar normal was maintained without interruptions. Many dislocations were found in the form of discontinuities in the fringes as pointed out by arrows in the figure. The curved fringes may be the product of either a combination of lattice spacing differences and rotation or of varying rotations, with the latter being most probable.

Conclusion

In summary, we have attempted to understand the ripple formation mechanism in the s-PP lamellar single crystals grown from the melt in thin films observed previously in TEM[5] and AFM measurements at high temperatures in this study. The ripples must be associated with the chain orientation variations in different growth sectors of the crystals. Using two DF imaging techniques, we found that in the (100) sectors a periodic sinusoidal-like orientation variation of the *c*-axis in the crystals was displayed along the longitudinal axis (the crystal *b*-axis) direction of the lamellar crystal. The bright streaks found in the (020) DF image were associated with the ripples. In the (200) DF images, modulation of the orientation in the longitudinal axis direction in the (100) sectors was less clear but was still discernible. It was deduced that the crystal *c*-axis orientation in the (100) sectors deviated along both the transverse and the longitudinal directions of the lamellar crystal, and the deviations were primarily along the longitudinal axis direction. A possible mechanism of the ripple formation is proposed. This is due to the major contractions along the longitudinal axis direction caused by the lamellar thickening in the (010) sectors during the crystal growth. The chain orientation can be further deduced using Moiré fringes. Moiré patterns were observed in the (010) sectors of superimposed crystals in the (020) DF images while no Moiré patterns were found in the (100) sectors based on the (020) DF images. On the other hand, Moiré patterns in the (200) DF images only exhibited randomized fringe patterns except to some local extent in the overlapped (100) sectors. These peculiar DF images and Moiré fringes may also be influenced by overlapping of the (010) sector of one crystal with the (100) sector of another. Furthermore, results from the Moiré patterns of the (020) and (200) DF images suggest that in the (010) sectors the deviation of the crystal *c*-axis from the lamellar normal may be mainly toward the longitudinal axis direction. The (220) DF images exhibited continuously curved fringes, revealing that the crystal *c*-axis orientation in the (110) planes in both sectors does not differ abruptly across the sector boundaries.

Acknowledgment. S.Z.D.C. acknowledges support by the NSF (DMR-0203994) and Phillips Petroleum Co. The authors thank Dr. Freddy Khoury at National Institute of Standard and Technology and Professor Christopher Y. Li at Drexel University for their very thoughtful discussions and comments.

References and Notes

(1) Lotz, B.; Lovinger, A. J.; Cais, R. E. *Macromolecules* **1988**, *21*, 2375.
(2) Lovinger, A. J.; Lotz, B.; Davis, D. D. *Polymer* **1990**, *31*, 2253.
(3) Lovinger, A. J.; Davis, D. D.; Lotz, B. *Macromolecules* **1991**, *24*, 552.
(4) Lovinger, A. J.; Lotz, B.; Davis, D. D.; Padden, F. J., Jr. *Macromolecules* **1993**, *26*, 3494.

(5) Lovinger, A. J.; Lotz, B.; Davis, D. D.; Schumacher, M. *Macromolecules* **1994**, *27*, 6603.
(6) Tsukruk, V. V.; Reneker, D. H. *Macromolecules* **1995**, *28*, 1370.
(7) Bu, Z.; Yoon, Y.; Ho, R.-M.; Zhou, W.; Jangchud, I.; Eby, R. K.; Cheng, S. Z. D.; Hsieh, E. T.; Johnson, T. W.; Geerts, R. G.; Palackal, S. J.; Hawley, G. R.; Welch, M. B. *Macromolecules* **1996**, *29*, 6575.
(8) Lotz, B.; Mathieu, C.; Thierry, A.; Lovinger, A. J.; De Rosa, C.; Ruiz de Ballesteros, O.; Auriemma, A. *Macromolecules* **1998**, *31*, 9253.
(9) Rodriguez-Arnold, J.; Zhang, A.; Cheng, S. Z. D.; Lovinger, A. J.; Hsieh, E. T.; Chu, P.; Johnson, T. W.; Honnell, K. G.; Geerts, R. G.; Palackal, S. J.; Hawley, G. R.; Welch, B. *Polymer* **1994**, *35*, 1884.
(10) Rodriguez-Arnold, J.; Bu, Z.; Cheng, S. Z. D.; Hsieh, E. T.; Johnson, T. W.; Geerts, R. G.; Palackal, S. J.; Hawley, G. R.; Welch, B. *Polymer* **1994**, *35*, 5194.
(11) Zhou, W.; Cheng, S. Z. D.; Eby, R. K.; Reneker, D.; Lotz, B.; Hsieh, E. T.; Johnson, T. W.; Geerts, R. G.; Palackal, S. J.; Hawley, G. R.; Welch, M. B. *Macromolecules* **2000**, *33*, 6861.
(12) De Rosa, C.; Corradini, P. *Macromolecules* **1993**, *26*, 5771.
(13) De Rosa, C.; Auriemma, A.; Vinti, V. *Macromolecules* **1998**, *31*, 7430.
(14) Lacks, D. J.; Rutledge, G. C. *Macromolecules* **1995**, *28*, 5789.
(15) Kyu, T. Private discussions.
(16) Kobayashi, K. *Kagaku (Chem.)* **1962**, *8*, 203.
(17) Lovinger, A. J.; Keith, H. D. *J. Polym. Sci., Polym. Phys. Ed.* **1981**, *19*, 1163.
(18) Okihara, T.; Cartier, L.; Alberda van Elenstein, G. O. R.; Lotz, B. *Polymer* **1999**, *40*, 1.
(19) Agar, A. W.; Frank, F. C.; Keller, A. *Pill. Mag.* **1959**, *4*, 32.
(20) Holland, V. F. *J. Appl. Phys.* **1964**, *35*, 3235.
(21) Bassett, D. C. *Pill. Mag.* **1964**, *10*, 595.
(22) Hirsch, P. B.; Howie, A.; Nicholson, R. B.; Pashley, D. W.; Whelan, M. J. *Electron Microscopy of Thin Crystals*; Butterworth: London, 1965.
(23) Williams, D. B.; Carter, C. B. *Transmission Electron Microscopy: A Textbook for Materials Science*; Plenum Press: New York, 1996.

MA030312X